

## Experimental testing on semi-active vibration control through adaptive structural joints

Wang, Qinyu; Senatore, Gennaro ; Jansen, K.M.B.; Habraken, Arjan; Teuffel, Patrick

**Publication date**

2021

**Document Version**

Final published version

**Published in**

Proceedings of the IASS Annual Symposium and Spatial Structures Conference 2020/21, 23-27 August 2021, Guilford, UK

**Citation (APA)**

Wang, Q., Senatore, G., Jansen, K. M. B., Habraken, A., & Teuffel, P. (2021). Experimental testing on semi-active vibration control through adaptive structural joints. In S. A. Behnejad, G. A. R. Parke, & O. A. Samavati (Eds.), *Proceedings of the IASS Annual Symposium and Spatial Structures Conference 2020/21, 23-27 August 2021, Guilford, UK* IASS.

**Important note**

To cite this publication, please use the final published version (if applicable).  
Please check the document version above.

**Copyright**

Other than for strictly personal use, it is not permitted to download, forward or distribute the text or part of it, without the consent of the author(s) and/or copyright holder(s), unless the work is under an open content license such as Creative Commons.

**Takedown policy**

Please contact us and provide details if you believe this document breaches copyrights.  
We will remove access to the work immediately and investigate your claim.

## Experimental testing on semi-active vibration control through adaptive structural joints

Qinyu WANG<sup>\*a</sup>, Gennaro SENATORE<sup>b</sup>, Kaspar JANSEN<sup>c</sup>, Arjan HABRAKEN<sup>a</sup>, Patrick TEUFFEL<sup>a</sup>

<sup>a</sup> Chair of Innovative Structural Design (ISD), TU Eindhoven, 5600MB Eindhoven, NL, q.wang2@tue.nl

<sup>b</sup> Applied Computing and Mechanics Laboratory (IMAC, ENAC); Swiss Federal Institute of Technology (EPFL)

<sup>c</sup> Department of Design Engineering, TU Delft, 2628 CE Delft, NL

### Abstract

This paper presents experimental testing of a new type of semi-active variable stiffness and damping control device in the form of an adaptive joint for truss and frame structures. The adaptive joint is made of a shape memory polymer (SMP) core that is reinforced by a SMP-aramid skin. Actuation through resistive heating transitions the SMP core material from a glassy to a rubbery state, which causes a significant stiffness reduction and a parallel increase of damping due to viscoelastic effects. Experimental testing on a 1325 mm x 650 mm x 650 mm three-floor frame is carried out to investigate the capabilities of this new semi-active control device to mitigate the structure dynamic response. The prototype frame is made of 30 aluminum tube elements connected through 12 adaptive joints which have been 3D printed. Stiffness and damping characteristics are controlled independently through PID control using a temperature sensor and a resistive heating wire which are embedded in the core of each joint. A free vibration test is carried out to measure the structure natural frequency and damping change from ambient (25°C) to the transition temperature (65°C). The fundamental frequency shift (reduction) is 27.4% while the structure damping ratio increases from 2.6% to 8.0%. Such a frequency shift and increase of damping allows for a significant reduction of the dynamic response under base excitation. Through thermal actuation of the joints to the transition temperature, acceleration and displacement responses under base excitation reduce by 88% and 78%, respectively.

**Keywords:** adaptive structures, semi-active control, vibration control, variable stiffness, variable damping, viscoelastic, frequency shift, structural dynamics

## 1. Introduction

### 1.1. Previous work

Adaptive structures are able to maintain optimal performance under changing loading conditions through sensing, actuation and control. Structural control strategies have been categorized into four main types: passive, active, semi-active, and hybrid (Soong and Spencer [1]). Passive control systems (e.g. base isolation as in Huang *et al.* [2], viscoelastic and elastoplastic dampers as in Kasai *et al.* [3]) require no control power, but they have limited capabilities compared to active and semi-active systems. Active control has been applied to seismic (Spencer *et al.* [4], Ohtori *et al.* [5]) and wind excited (Yang *et al.* [6]) buildings in order to reduce the structure response (e.g. displacement, acceleration, and inter-story drift). Active control systems are more effective to suppress vibrations than passive control systems. However, active systems generally require high power density supply and due to the complexity of the control model, instability of the structure-control system might arise due to uncertainty and/or modelling inaccuracy (Kinay and Turan [7], Wang *et al.* [8]). Semi-active control systems (e.g. magnetorheological dampers) maintain some of the capabilities of active systems while requiring less energy and are as reliable as passive systems (Harvey *et al.* [9], Symans and Constantinou [10]). Hybrid control systems

(e.g. hybrid mass dampers) combine the advantages of passive, semi-active and active control strategies and devices, but they are generally complex and might involve significant maintenance costs (Gkatzogias and Kappos [11]).

By actively counteracting the effect of external loads through control of internal forces and the external geometry, adaptive structures have been designed to operate with a better material utilization (Teuffel [12]) and a lower whole-life energy (Senatore *et al.* [13]) than conventional passive structures. The whole-life energy comprises an embodied part in the material and an operational part for adaptation to loading. Extensive numerical (Senatore *et al.* [14, 15]) and experimental studies (Senatore *et al.* [16]) have shown that when the design is stiffness governed, up to 70% of the whole-life energy can be saved by well-designed adaptive structures compared to weight-optimized passive structures. Structural adaptation involves shape changes that require flexibility of the joints during control to prevent stress build-up which could lead to a lower control accuracy and an increase of control effort. To address this challenge, adaptive joints with variable stiffness properties have been proposed in previous own work Senatore *et al.* [17]. The joint transitions from a “locked” to a “released” state (moment to pin connection) via a stiffness reduction which is caused by a controlled change of material properties through actuation (Wang *et al.* [18]).

Shape memory polymers (SMPs) have received attention for applications as actuators in deployable and morphing structures because of their variable stiffness and shape recovery properties (Liu *et al.* [19]). However, SMPs’ low mechanical strength limits applications in load-bearing structures. SMPs reinforced by continuous fibers (e.g. carbon, glass and aramid fibers) have a significantly increased mechanical strength in the fiber direction while keeping the shape memory effect in the transverse direction (Lan *et al.* [20], Gall *et al.* [21]). Generally, fiber reinforced SMP composites are more suitable for application in load-bearing structures (Liu *et al.* [19], Hu *et al.* [22]). Previous own work Wang *et al.* [18] has investigated an adaptive joint made of a polyurethane based shape memory polymer (SMP) core reinforced by an SMP-aramid skin. The joint has been actuated thermally through a heating wire embedded in the SMP core. The change from a glassy to a rubbery state that occurs when the joint is actuated to the transition temperature ( $T_g = 65^\circ\text{C}$ ), causes a significant stiffness reduction and a parallel increase of material damping.

Thanks to the variable stiffness and damping properties, such adaptive joints can function as a new type of semi-active control device. With respect to existing semi-active variable stiffness and damping devices (Kobori *et al.* [23], Sarlis *et al.* [24], Shu *et al.* [25]), the system proposed in this work is much better integrated since the joint functions as a structural component as well as a semi-active control device that does not require complex detailing for installation. For structures equipped with such variable stiffness and damping joints, it is possible to cause a significant frequency shift and increase of the damping ratio solely through actuation of the joints, which can be employed as a strategy to mitigate the dynamic response. Numerical simulations have been carried out on a truss bridge subjected to a resonance and a moving load as well as a four-story frame subjected to El Centro earthquake loading (Wang *et al.* [26]). Both structures are equipped with variable stiffness and damping joints at all nodes (7 for the truss bridge and 8 for the multi-story frame). Through thermal actuation of the joints in the range  $50\text{-}60^\circ\text{C}$ , the average acceleration and displacement response reduce by up to 95% and 20% for the truss bridge and 47% and 46% for the four-story frame.

## **1.2. Outline**

The remainder of this paper is arranged as follows. Section 2 gives details of a three-floor frame equipped with 12 adaptive joints, including thermal actuation and control system. Section 3 presents a quantitative study that evaluate frequency shift and damping variation of the three-floor frame through thermal actuation of the joints. Section 4 presents numerical and experimental studies on semi-active vibration control of the three-floor frame subjected to sinusoidal base excitation. Sections 5 and 6 conclude the paper.

## 2. Design of the prototype

### 2.1. Aluminum frame equipped with 12 adaptive joints

The prototype structure is a 1325 mm x 650 mm x 650 mm three-floor frame. Figure 1 shows the structure elevation from two sides indicated by the plane  $xz$  in (a) and the plane  $yz$  in (b). Figure 1 (c) shows a picture of the physical prototype. The structure is made of 30 aluminum tube elements connected through 12 adaptive joints. All aluminum tubes have an outer diameter of 25 mm and a wall thickness of 5 mm. Each joint core has been fabricated through 3D printing. When the joint core is actuated to a temperature above 50°C, pronounced deformations of the core might occur due to loading. Therefore, an SMP-aramid composite skin has been applied to reinforce the joint core and its connection to the tube elements. This skin consists of a stack of woven aramid fabric layers which are impregnated with SMP material to form a stiff and thin composite. Four individual fabric layers with orientations of the fibers at 0°, 45°x2, 90° are stacked to obtain a quasi-isotropic material that can take forces from multiple directions including those caused by bending and torsion. The reader is referred to Wang *et al.* [18] for further details regarding the adaptive joint core and the SMP-aramid reinforcement skin.

A mass of 20 kg is applied on each floor. The frame is subjected to one-dimensional ground motion (in the  $x$  direction) generated by a linear actuator (T60 actuator and BGM09 belt gear, *Thomson*; AKM42E-ANCNC-00 BLDC motor, *National Instruments*) which is connected directly to a shaking table mounted on a rail system. Diagonal bracings are installed only on the sides that lie in the plane  $yz$  to limit torsional effects. Ground acceleration and displacement are measured by an accelerometer (BDK3, *seika.de*) and a draw-wire displacement sensor (500-FD60, *Altheris*) which are located on the left side of the shaking table. Additional three accelerometers are installed in the middle of left side beams for each floor to measure accelerations in the  $x$  direction. The accelerometers are indicated by red square marker in Figure 1 (a) and (b). Two strain sensors are installed in a full-bridge configuration (1-XY33-3/350, *HBM*) to the middle of two first-floor columns in order to measure the axial stress. Additional two strain gauges are installed in a quarter-bridge configuration (PEL-10-11, *Tokyo Sokki Kenkyujo*) to the support end of the same columns in order to measure the bending stress. The strain gauges are indicated by a blue square marker in Figure 1 (a). A real-time target machine (NI cRIO-9038, *National Instruments*) is employed to control the linear actuator motion, to measure the joint temperature, and to modulate power supply for heating the joints. A data acquisition system (cDAC-9178, *National Instruments*) system is employed to monitor the structure response which is measured through the accelerometers and strain sensors.

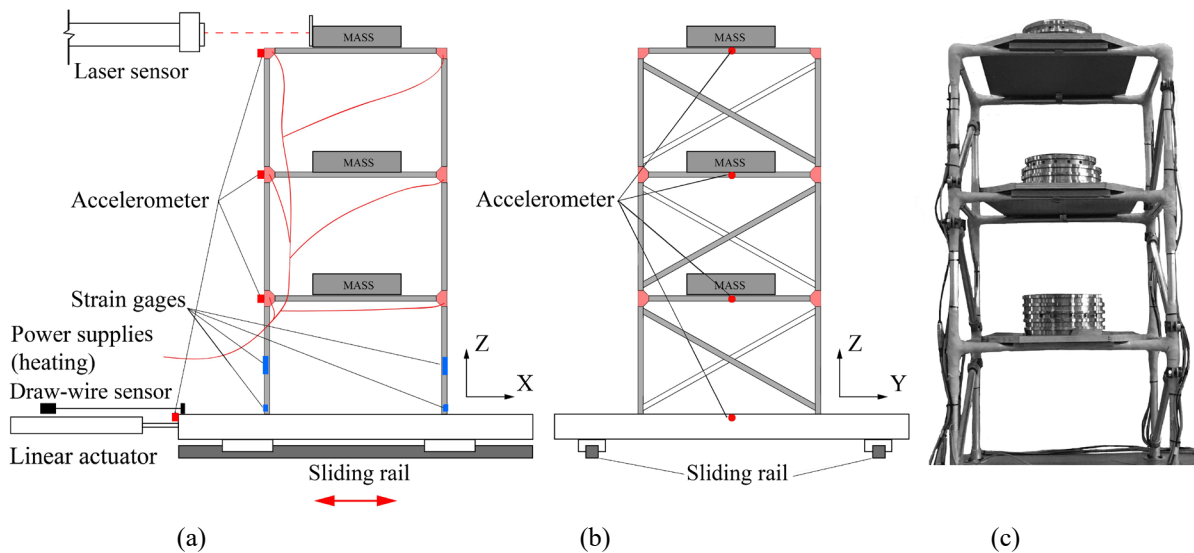


Figure 1: (a) and (b): elevation  $xz$  and  $yz$  of the frame structure; (c) experimental prototype

## 2.2. Temperature control system

Figure 2 shows one of the joints without (a) and with (b) SMP-aramid reinforcement skin. A resistive heating wire is embedded in the core of each joint. The lengths of the embedded heating wires are approximately 1.8 m for the four joints of the top floor which connect 3 elements each and 2.2m for the other joints which connect 4 elements each.

Stiffness and damping characteristics of the 12 adaptive joints are controlled independently through PID control. Figure 2 (c) shows 12 solid-state relays (DC60S5, *Crydom*) which are controlled by the real-time controller to modulate power supply to the heating wire embedded in each joint. A resistance temperature detector (RTD) (F2020-100-A, *Omega*) is installed at the end of the heating wire to control the thermal flux to each joint. Two power supplies (230V/12VDC, 350W, *Schloss*) are employed for thermal actuation. Considering a 12VDC power supply, the working power rates of the 1.8 m and 2.2 m heating wires are 57 W and 46 W, respectively.

A thermocouple is installed to monitor the surface temperature of each joint. Temperature measurements are logged through a multi-channel data logger (Squirrel 2040, *Grant*).

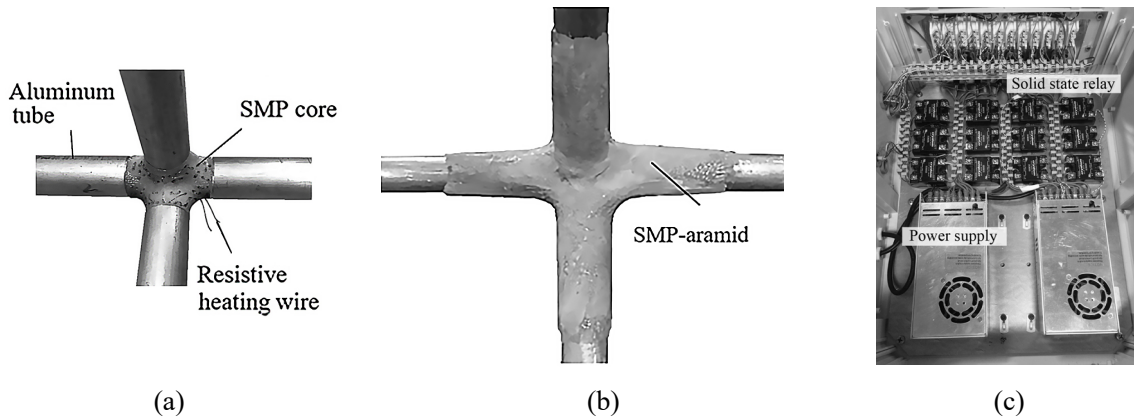


Figure 2: (a) SMP core connected to four aluminum tubes; (b) SMP-aramid reinforcement skin;(Wang *et al.* [26]) (c) solid state relays and power supplies

## 3. Frequency shift and damping variation

### 3.1. Numerical model

The SMP material of the joint core was characterized through a dynamic mechanical analysis (DMA) test which is described in previous own work Wang *et al.* [18]. Figure 3 shows the plot of storage modulus  $E'$ , loss modulus  $E''$  and  $\tan \delta$  as functions of the temperature at 1 Hz. The storage modulus is the elastic stiffness while the loss modulus is the energy dissipated through heat due to friction. The ratio  $\tan \delta = E''/E'$  is a measure of the material mechanical damping. Through an increase of temperature, the material transitions from a glassy to a rubbery state via a viscoelastic region. The glass transition temperature is 65°C. During glass transition (50°C to 65°C), the elastic stiffness reduces by 96% while damping increases 11-fold. A master curve that characterizes the viscoelastic material behavior was obtained from testing in the temperature-frequency domain 40 °C to 85 °C, 0.3 Hz to 32 Hz (Wang *et al.* [18]). The SMP-aramid reinforcement skin material is assumed to be temperature independent since the aramid fibers mechanical features are dominant. A modulus of 8320 MPa and an ultimate stress of 107 MPa is assumed as obtained from experimental measurement (Wang *et al.* [18]).

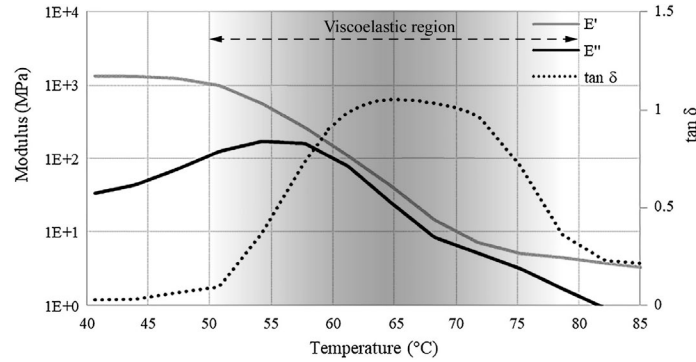


Figure 3: Storage modulus  $E'$ , loss modulus  $E''$  and  $\tan \delta$  obtained from dynamic mechanical analysis (DMA) test at 1 Hz (Wang *et al.* [26])

A simpler material model, which is here named “thermo-elastic”, is also considered by taking the storage modulus curve at 1 Hz (Figure 3) and ignoring damping variation due to viscoelastic effects. The thermo-elastic material model is employed for modal analysis and transient analysis through mode superposition. The viscoelastic material model is employed for full transient analysis. In both cases the objective is to evaluate the effect of joint stiffness variation (thermo-elastic) as well as combined stiffness and damping variation (viscoelastic) on the structure response under loading.

The frame structure is modelled through finite elements in Ansys workbench. Each aluminum tube is modelled with 9 beam elements (BEAM188) and each joint with approximately 2690 solid elements (SOLID186). The beam elements connect to the joint through a section perpendicular to their axis as indicated by the yellow contouring in Figure 4 (a). The beam sections connect to the joint elements through a fixed contact. The isotropic SMP-aramid skin is modelled with “surface coating” (SUPF156) elements with a thickness of 3 mm which is obtained by stacking 8 aramid fabric layers of the SMP-aramid composite described in Section 2.1.

### 3.2. Frequency shift and damping variation obtained through transient analysis

The 1<sup>st</sup> and 2<sup>nd</sup> modes are considered to evaluate natural frequency shift and modal damping variation caused by thermal actuation of the joints. Figure 4 shows the 1<sup>st</sup> and 2<sup>nd</sup> modal shapes. Natural frequency and frequency shift for 1<sup>st</sup> and 2<sup>nd</sup> modes are given in Table 2. Due to the stiffness reduction of the joints caused by thermal actuation from ambient to transition temperature (65 °C), the frequency for 1<sup>st</sup> and 2<sup>nd</sup> modes shifts significantly by 27.6% and 23.5%, respectively.

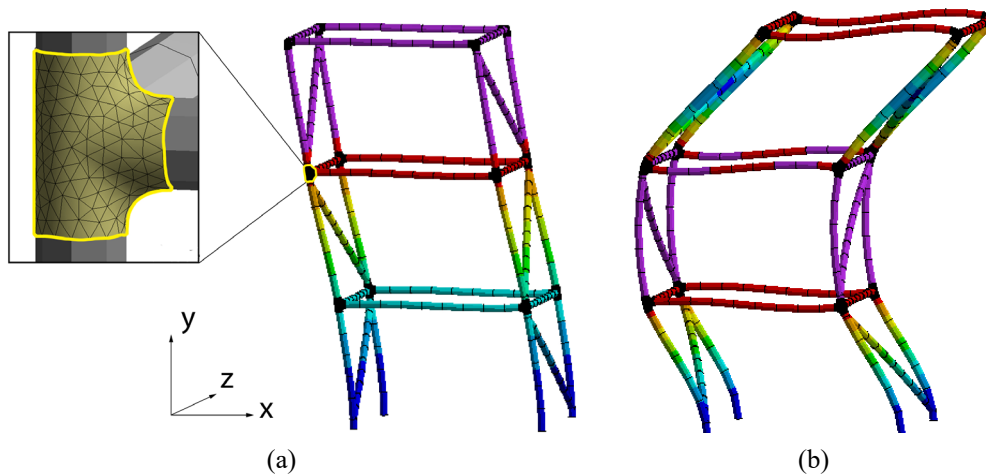


Figure 4: (a) and (b): modal shapes of 1<sup>st</sup> and 2<sup>nd</sup> modes

The viscoelastic material model is employed to simulate the structure free vibration within a time period of 10s (temperature range from 40 °C to 65 °C). Free vibration is caused by a 1N impulse load in the x direction applied to the middle of the top floor left side beam. The damping ratio  $\zeta$  are computed from the logarithmic decrement  $\Delta = \ln (u_t/u_{t+1})$  as:

$$\zeta = \frac{\Delta/2\pi}{\sqrt{1+(\Delta/2\pi)^2}} \quad (1)$$

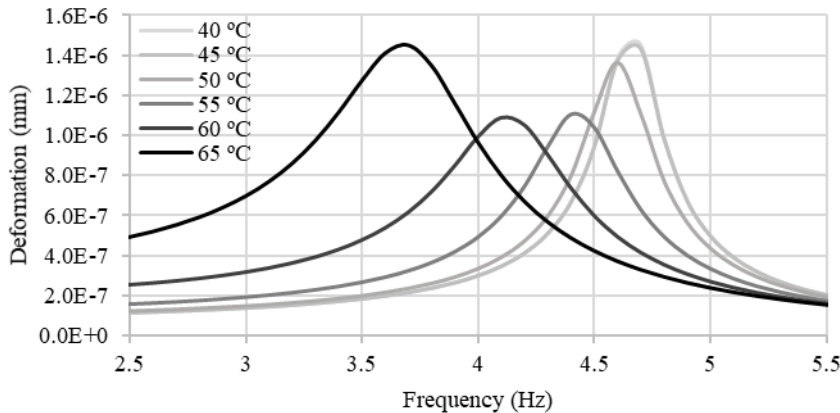
where u is the peak amplitude of the average displacement among all degrees of freedom of the top floor, which is here denoted as ‘deformation’ for brevity.

In each analysis the joints are assumed to be actuated through resistive heating from ambient 25°C to transition temperature 65°C in discrete steps of 5°C. At ambient temperature (25°C), the structure damping is set to 2.6% which has been measured from a free vibration measurement (see Section 4). The damping ratios  $\zeta$  for the other temperatures, given in Table 1, are obtained through full transient analysis using the viscoelastic material model. The damping ratio increases from 2.6% at 25°C to 8.4% when the joints are actuated to 65°C. The effect of material viscoelasticity significantly increases the structure damping by 5.8%.

Figure 5 (a) and (b) show the deformation vs frequency curves for the 1<sup>st</sup> and 2<sup>nd</sup> mode, respectively, which have been obtained through Fast Fourier transform (FFT). As expected, the natural frequency (corresponding to the deformation peak values) shifts to left when the joints are actuated from 40°C to 60°C, which is caused by the stiffness reduction. At 40°C, the 1<sup>st</sup> modal frequencies computed through modal analysis and FFT are 4.6 Hz and 4.7 Hz, respectively. For the 2<sup>nd</sup> mode, the frequencies computed through modal analysis and FFT are 15.0 Hz and 14.4 Hz, respectively. The difference in percentage terms is 2.8% and 4% for the 1<sup>st</sup> and 2<sup>nd</sup>, respectively. At 65°C, this difference reaches a maximum value of 10.8% for the 1<sup>st</sup> modal frequency (3.3 Hz from modal analysis and 3.7 Hz from FFT), and is 11.2% for the 2<sup>nd</sup> modal frequency (11.6 Hz from modal analysis and 12.9 Hz from FFT).

Table 1: frequency shift for 1<sup>st</sup> and 2<sup>nd</sup> mode and damping ratio obtained modal analysis

	25 °C	30 °C	35 °C	40 °C	45 °C	50 °C	55 °C	60 °C	65 °C
$\omega_1$ (Hz)	4.62	4.61	4.59	4.57	4.55	4.46	4.16	3.74	3.34
$\omega_2$ (Hz)	15.2	15.1	15.0	15.0	14.9	14.7	13.8	12.7	11.6
$S_{\omega_1}$ (%)	-	0.3	0.7	1.1	1.5	3.4	10.0	19.1	27.6
$S_{\omega_2}$ (%)	-	0.7	1.0	1.4	1.7	3.4	9.1	16.7	23.5
$\zeta$ (%)	2.6	-	-	2.8	2.8	3.5	5.0	6.0	8.4



(a)

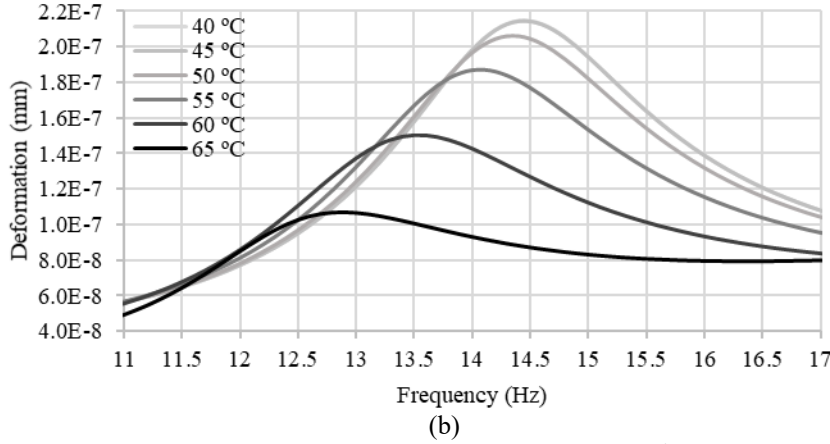


Figure 5. (a) and (b) deformation vs frequency from FFT for 1<sup>st</sup> mode and 2<sup>nd</sup> mode, viscoelastic material model

### 3.3. Frequency shift and damping variation measured through a free vibration test

Frequency shift and damping variation obtained from simulation are benchmarked against results measured through a free vibration test. An impulse force is applied on the left side of the top floor. The free vibration is recorded through the accelerometers (see 2.1) for a period of 100s. For each temperature, the measurement is repeated three times. The 1<sup>st</sup> and 2<sup>nd</sup> modal frequencies are obtained through Fast Fourier Transform (FFTs) of the recorded acceleration which is averaged over the three measurements. The frequency shifts are given in Table 2. In good accordance with numerical predictions, the frequency shifts from 25 °C and 65 °C for 1<sup>st</sup> and 2<sup>nd</sup> modes are 27.4% and 26.2%, respectively. However, the measured frequency shift is significantly higher than the corresponding value obtained from simulation at all other temperatures. The maximum discrepancy between numerical and experimental results occurs for the 1<sup>st</sup> mode at 50 °C (14.5% experimental vs 3.4% as obtained from simulation). Referring to Figure 3, the joint core material enters the viscoelastic region at approximately 50 °C at which storage modulus and material damping start to vary significantly. The joint temperature is measured through thermocouples installed on the surface. Therefore, the actual temperature in the core is expected to be higher, which explains a lower frequency (higher frequency shift) measured experimentally compared to numerical predictions. As the temperature reaches 60 °C - 65 °C, the storage modulus is less sensitive to temperature variation and therefore the difference between simulation and measurement reduces.

Table 2: frequency shift for 1<sup>st</sup> and 2<sup>nd</sup> mode and damping ratio obtained from experimental testing

	25 °C	30 °C	35 °C	40 °C	45 °C	50 °C	55 °C	60 °C	65 °C
$\omega_1$ (Hz)	4.63	4.53	4.38	4.26	4.08	3.96	3.78	3.6	3.36
$\omega_2$ (Hz)	16.2	15.8	15.3	14.9	14.3	14.0	13.2	12.8	12.0
$S_{\omega_1}$ (%)	-	2.2	5.4	8.0	11.9	14.5	18.4	22.2	27.4
$S_{\omega_2}$ (%)	-	2.4	5.4	8.3	11.5	13.8	18.3	21.0	26.2
$\zeta$ (%)	2.6	-	-	3	3.5	4.5	5.2	5.9	8.0

Variation of the damping ratio is obtained through FFT of the top floor displacement which is measured with a laser sensor (M5L-200 from MEL Mikroelektronik GmbH). Since the amplitudes of the free vibration peaks are very small and damp out very fast, the damping ratio  $\zeta$  is computed through the half-power bandwidth method (Butterworth *et al.* [27]) as:

$$\zeta = \frac{f_{res}(f_1 - f_2)}{(f_1^2 + f_2^2)} \quad (2)$$

where  $f_{res}$  is the frequency corresponding to the peak and  $f_1$  and  $f_2$  are the frequencies corresponding to half power amplitude ( $f_{res}/\sqrt{2}$ ). It is assumed that half of the total power is dissipated between  $f_1$  and  $f_2$ . The damping ratios  $\zeta$  are given in Table 2. Figure 6 gives an example of the half-power bandwidth method applied to compute the damping ratio at 65 °C.

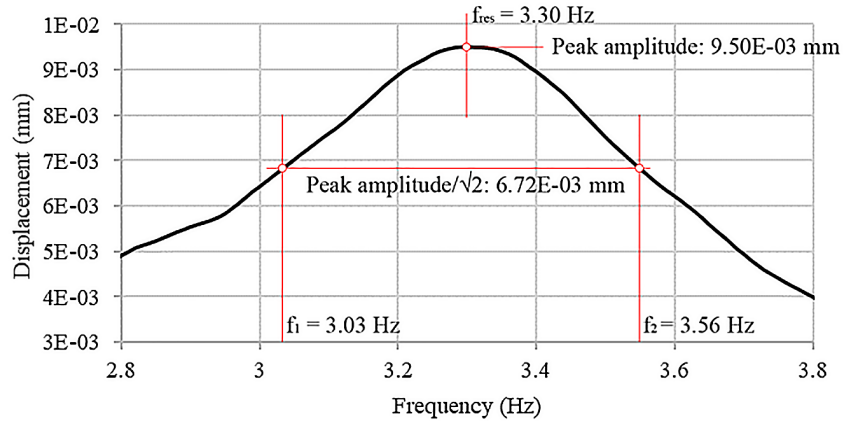


Figure 6: half-power bandwidth frequencies from displacement spectrum for 1<sup>st</sup> mode at 65°C

In good accordance with numerical predictions, the measured damping ratio increases from 2.6% to 8.0% when the joints are actuated from ambient to transition temperature 65 °C. The effect of material viscoelasticity increases significantly the damping ratio by 5.4%. However, the damping ratio measured experimentally is higher than that obtained through simulation from ambient to 55 °C. The maximum discrepancy between numerical predictions and measured values is 28% at 50 °C. Similar to what observed for the frequency shift, since the joint core temperature is higher than the surface temperature measured by thermocouple, a higher damping ratio is measured experimentally in the viscoelastic region compared to numerical predictions. As the temperature reaches 60 °C - 65 °C, material damping is less sensitive to temperature variation and therefore the difference between simulation and measurement reduces.

#### 4. Vibration control under sinusoidal base excitation

Semi-active control of vibrations through thermal actuation of variable stiffness and damping joints has been evaluated through numerical simulations and experimental testing. The prototype structure is subjected to a sinusoidal base excitation caused by motion of the linear actuator. The dynamic response is evaluated as the as the joints are actuated from ambient 25°C to transition temperature 65°C in discrete steps. For experimental testing, the joint temperature is set through PID control using feedback from thermocouples installed on the surface of each joint. Sufficient time is given so that the joint temperature stabilizes to the set value prior application of the base excitation. For numerical analysis, a constant thermal load is applied to the joint elements, which is increased in discrete steps.

The base excitation has a frequency of 4.4 Hz, an amplitude of 0.5 mm and it is applied for a period of 10s. Note that the 1<sup>st</sup> modal frequency measured through the free vibration test is 4.63 Hz. However, it was found through testing that the 1<sup>st</sup> mode is excited when the base excitation frequency is set to 4.4 Hz. This difference is likely to be attributed to some degree of looseness in the connections between the diagonal bracings and columns, between the plates that house the dead load and the floor beams, and the connections between the frame and the shaking table.

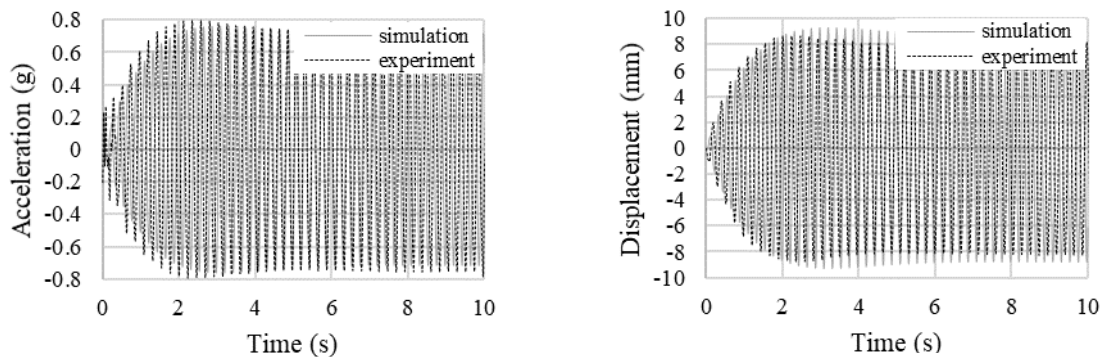
The dynamic response is also evaluated through transient analysis based on mode superposition, which is adopted in this case, instead of full transient analysis, because it offers a simple way to simulate a base excitation. When mode superposition is employed, the joint material model can only be the thermo-elastic model described in 3.1. However, to simulate damping variation caused by thermal actuation of

the joints, the structure damping ratio for each temperature is set to the damping ratio obtained from the free vibration test simulation (based on the viscoelastic material model).

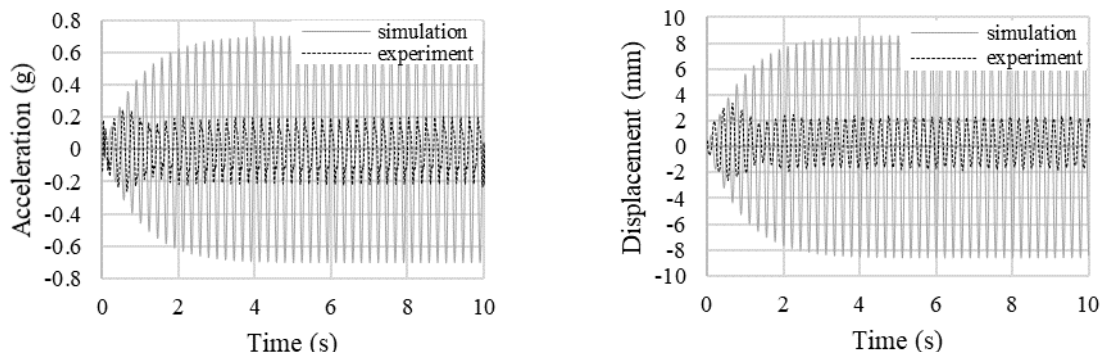
The top-floor acceleration and displacement are considered. The acceleration and displacement are measured by an accelerometer and a laser sensor which are indicated in Figure 1. Figure 7 shows the plot of top-floor acceleration and displacement vs time for the joints actuated at 25 °C, 50°C, and 65 °C. Accelerations and displacements of first and second floors are similar to that of the top floor, albeit of smaller amplitude, and therefore for brevity are not given.

Results from experimental testing and simulation show that, the top-floor acceleration decreases from 0.8 g to 0.1 g and the displacement decreases from 9 mm to 2 mm when the joints are actuated from 25 °C to 65 °C. However, at 50 °C the dynamic response obtained from simulation is much larger than that measured from experimental testing. Under resonance conditions, the effect of frequency shift on acceleration and displacement is dominant. As shown in Table 1 and Table 2, the 1<sup>st</sup> mode frequency shift at 50 °C is 14.5% from experimental testing while it is only 3.4% from simulation. A larger frequency shift causes a greater reduction of acceleration and displacement as measured from testing compared to simulation results. The same applies when the joints are actuated to 40 °C and 45 °C, because the measured frequency shift at these temperatures is larger than that obtained from simulation. When the joints are actuated to 60 °C and 65 °C, frequency shift and damping ratio increase are large in both cases (testing and simulation) and therefore the dynamic response reduces significantly. Thus, the recommended control temperature ranges from 60 °C to 65 °C.

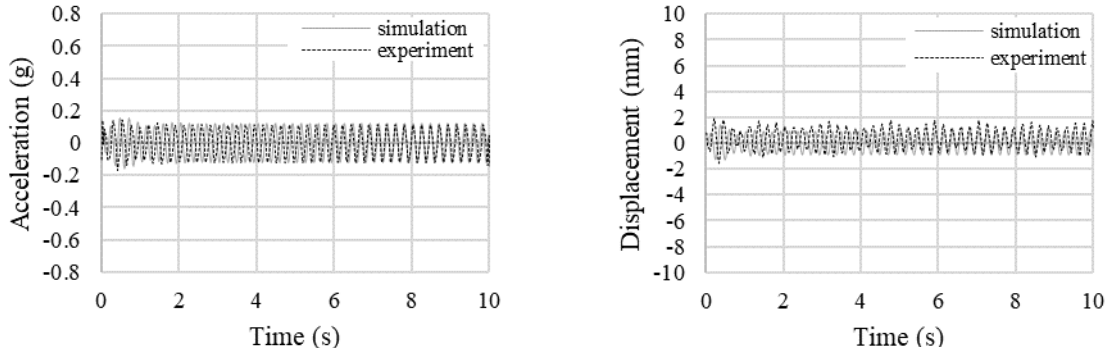
Figure 8 shows the reduction of the amplitude of the top-floor displacement taken from a video demonstration at 25 °C, 50°C, and 65 °C. The video demonstration is available as supplementary documentation.



(a) 25 °C



(b) 50 °C



(c) 65 °C

Figure 7: (a), (b) and (c) numerical and experimental results of top-floor acceleration and displacement vs time at 25°C, 50°C, and 65°C

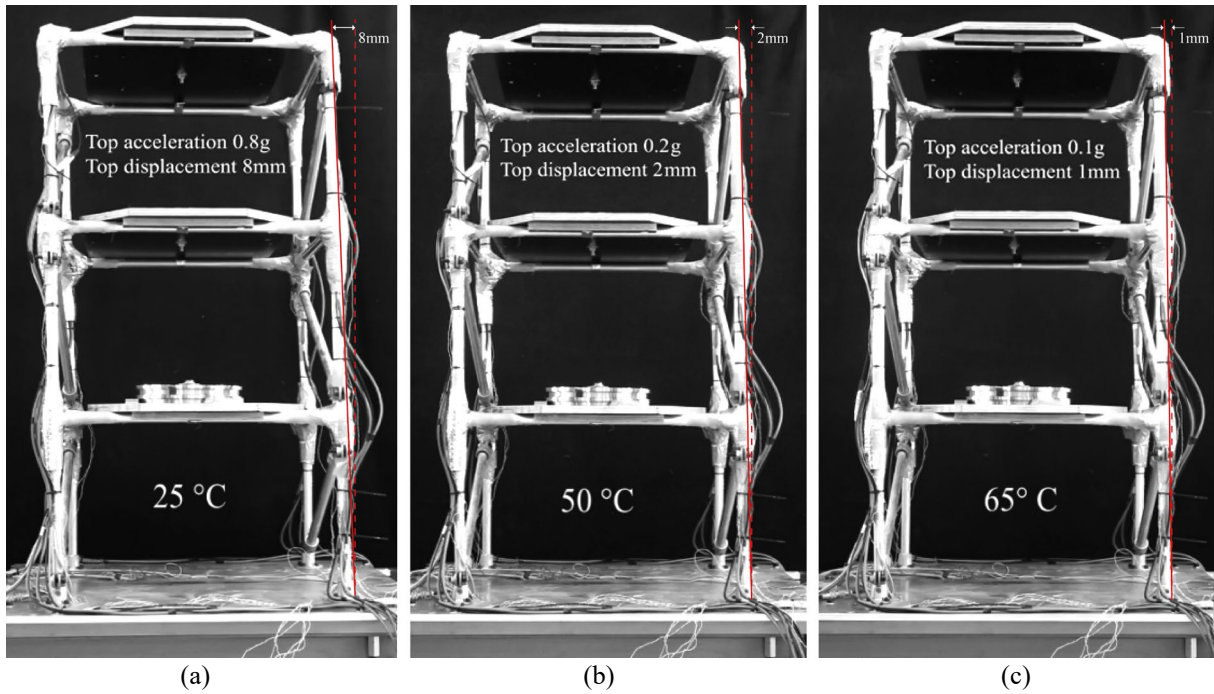


Figure 8: (a), (b) and (c) measured displacement amplitude of the top floor at 25°C, 50°C, and 65°C

## 5. Discussion

This paper has presented numerical and experimental studies to investigate the capability of a new adaptive structural joint which works as a semi-active variable stiffness and damping control device. Such an adaptive joint comprises a shape memory polymer (SMP) core reinforced with an SMP-aramid composite skin. Through thermal actuation, the joint stiffness decreases and in parallel material damping increases due to viscoelastic effects. This causes a significant shift of structure natural frequency and an increase of damping which can be employed to mitigate the dynamic response.

Numerical and experimental studies have been carried out on a three-floor frame prototype equipped with 12 adaptive joints. The structure natural frequency and damping variations caused by thermal actuation of the joints from ambient (25°C) to transition temperature (65°C) have been evaluated

through a free vibration test. Experimental and simulation results are in good accordance. The fundamental frequency shift is 27.4% between 25°C and 65°C. The damping ratio increases by 5.4% from 2.6% at 25°C to 8.0% 65°C. This allows for a significant reduction of the dynamic response under sinusoidal based excitation. The maximum acceleration and displacement of the top floor reduce by 88% (from 0.8g to 0.1g) and by 78% (from 9mm to 2mm), respectively.

A significant difference between experimental and simulation results has been observed for temperatures in proximity of the start (50 °C) of the viscoelastic region. The joint temperature is measured through thermocouples installed on the surface. Therefore, the actual temperature in the core is expected to be higher, which explains a larger frequency shift and damping increase measured experimentally compared to numerical predictions. As the temperature reaches 60 °C - 65 °C, storage modulus and damping ratio are less sensitive to temperature variation (see Figure 3) and therefore the difference between simulation and measurement reduces.

## **6. Conclusion**

A new adaptive structural joint has been tested which seamlessly combine two functions: structural joint and semi-active variable stiffness and damping control device. Simulation and experimental testing on a three-floor frame prototype equipped with 12 adaptive joints have shown that this new semi-active control strategy is effective to mitigate the dynamic response caused by based excitation.

In order to generalize the conclusion reached in this paper, future work will test semi-active control through thermal actuation of variable stiffness and damping joints under earthquake loading. Fatigue and control time delays due to heating and cooling of the joints will be also considered.

## **7. Acknowledgements**

This research project “Adaptive Joints with Variable Stiffness” has been supported by 4TU Lighthouse Projects 2017 (LHP2017) and China Scholarship Council (CSC).

## **8. References**

- [1] T. T. Soong and B. F. Spencer, "Active, semi-active and hybrid control of structures," *Bulletin of the New Zealand Society for Earthquake Engineering*, vol. 33, no. 3, pp. 387-402, 2000.
- [2] B. Huang, H. Zhang, H. Wang and G. Song, "Passive base isolation with superelastic nitinol SMA helical springs. Smart Materials and Structures," *Smart Materials and Structures*, vol. 23, no. 6, p. 065009, 2014.
- [3] K. Kasai, Y. Fu and A. Watanabe, "Passive control systems for seismic damage mitigation," *Journal of Structural Engineering*, vol. 124, no. 5, pp. 501-512, 1998.
- [4] B. F. Spencer Jr, R. E. Christenson and S. J. Dyke, "Next generation benchmark control problem for seismically excited buildings," in *Proceedings of the Second World Conference on Structural Control*, Kyoto, 1998.
- [5] Y. Ohtori, R. E. Christenson, B. F. Spencer Jr and S. J. Dyke, "Benchmark control problems for seismically excited nonlinear buildings," *Journal of Engineering Mechanics*, vol. 130, no. 4, pp. 366-385, 2004.
- [6] J. N. Yang, A. K. Agrawal, B. Samali and J. C. Wu, "Benchmark problem for response control of wind-excited tall buildings," *Journal of Engineering Mechanics*, vol. 130, no. 4, pp. 437-446, 2004.
- [7] G. Kınay and G. Turan, "A hybrid control of seismic response by passive and semi-active control strategies," *Journal of Engineering Science and Design*, vol. 2, no. 1, pp. 27-36, 2012.
- [8] L. Wang, X. Wang, Y. Li, G. Lin and Z. Qiu, "Structural time-dependent reliability assessment of the vibration active control system with unknown-but-bounded uncertainties," *Structural Control and Health Monitoring*, vol. 24, no. 10, p. e1965, 2017.

- [9] P. S. Harvey Jr, H. P. Gavin, J. T. Scruggs and J. M. Rinker, "Determining the physical limits on semi-active control performance: a tutorial," *Structural Control and Health Monitoring*, vol. 21, no. 5, pp. 803-816, 2014.
- [10] M. D. Symans and M. C. Constantinou, "Semi-active control systems for seismic protection of structures: a state-of-the-art review," *Engineering structures*, vol. 21, no. 6, pp. 469-487, 1999.
- [11] K. I. Gkatzogias and A. J. Kappos, "Semi-active control systems in bridge engineering: a review of the current state of practice," *Structural Engineering International*, vol. 26, no. 4, pp. 290-300, 2016.
- [12] P. Teuffel, "Entwerfen Adaptiver Strukturen," (Doctoral dissertation), University of Stuttgart - ILEK, Stuttgart, 2004.
- [13] G. Senatore, P. Duffour and P. Winslow, "Synthesis of Minimum Energy Adaptive Structures," *Structural and Multidisciplinary Optimization*, vol. 60, no. 3, pp. 849-877, 2019.
- [14] G. Senatore, P. Duffour and P. Winslow, "Energy and Cost Analysis of Adaptive Structures: Case Studies," *Journal of Structural Engineering (ASCE)*, vol. 144, no. 8, p. 04018107, 2018a.
- [15] G. Senatore, P. Duffour and P. Winslow, "Exploring the Application Domain of Adaptive Structures," *Engineering Structures*, vol. 167, pp. 608-628, 2018b.
- [16] G. Senatore, P. Duffour, P. Winslow and C. Wise, "Shape Control and Whole-Life Energy Assessment of an "Infinitely Stiff" Prototype Adaptive Structure," *Smart Materials and Structures*, vol. 27, no. 1, p. 015022, 2018c.
- [17] G. Senatore, Q. Wang, H. Bier and P. Teuffel, "The use of variable stiffness joints in adaptive structures," in *IASS 2017*, Hamburg, 2017.
- [18] Q. Wang, G. Senatore, K. Jansen, A. Habraken and P. Teuffel, "Design and characterization of variable stiffness structural joints," *Materials & Design*, vol. 187, p. 108353, 2020.
- [19] Y. Liu , H. Du, L. Liu and J. Leng, "Shape memory polymers and their composites in aerospace applications: a review," *Progress in Materials Science*, vol. 56, no. 7, pp. 1077-1135, 2011.
- [20] X. Lan, Y. Liu, H. Lv, X. Wang, J. Leng and S. Du, "Fiber reinforced shape-memory polymer composite and its application in a deployable hinge," *Smart Materials and Structures*, vol. 18, no. 2, p. 024002, 2009.
- [21] K. Gall, M. Mikulas, N. A. Munshi, F. Beavers and M. Tupper, "Carbon fiber reinforced shape memory polymer composites," *Journal of Intelligent Material Systems and Structures*, vol. 11, no. 11, pp. 877-886, 2000.
- [22] J. Hu, W. Chen, P. Fan, J. Gao, G. Fang, Z. Cao and F. Peng, "Uniaxial tensile tests and dynamic mechanical analysis of satin weave reinforced epoxy shape memory polymer composite," *Polymer Testing*, vol. 64, pp. 235-41, 2017.
- [23] T. Kobori, M. Takahashi, T. Nasu, N. Niwa and N. Ogasawara, "Seismic response controlled structure with Active Variable Stiffness system," *Earthquake Engineering and Structural Dynamics*, vol. 22, no. 1, pp. 925-941, 1993.
- [24] A. A. Sarlis, D. T. R. Pasala, M. C. Constantinou, A. M. Reinhorn, S. Nagarajaiah and D. P. Taylor, "Negative Stiffness Device for Seismic Protection of Structures," *Journal of Structural Engineering*, vol. 139, no. 7, 2013.
- [25] Z. Shu, J. Zhang and S. Nagarajaiah, "Dimensional Analysis of Inelastic Structures with Negative Stiffness and Supplemental Damping Devices," *Journal of Structural Engineering*, vol. 143, no. 3, 2017.
- [26] Q. Wang, G. Senatore, K. Jansen, A. Habraken and P. Teuffel, "Vibration suppression through variable stiffness and damping structural joints," *Frontiers in Built Environment*, vol. 6, p. 550864, 2020.
- [27] J. Butterworth, J. H. Lee and B. Davidson, "Experimental determination of modal damping from full scale testing," in *13th World Conference on Earthquake Engineering*, Vancouver, 2004.